Title

Harmonizing tau positron emission tomography in Alzheimers disease: The CenTauR scale and the joint propagation model.

Journal

Alzheimers & Dementia: The Journal of the Alzheimers Association, 20(9)

Authors

Leuzy, Antoine
Raket, Lars
Villemagne, Victor
et al.

Publication Date

2024-09-01

DOI

10.1002/alz.13908

Peer reviewed

Received: 7 November 2023 | Revised: 15 March 2024 | Accepted: 18 March 2024

DOI: 10.1002/alz.13908

Alzheimer's & Dementia®
THE JOURNAL OF THE ALZHEIMER'S ASSOCIATION

RESEARCH ARTICLE

Harmonizing tau positron emission tomography in Alzheimer's disease: The CenTauR scale and the joint propagation model

Antoine Leuzy[1,2,3] | Lars Lau Raket[1,4] | Victor L. Villemagne[5,6,7] | Gregory Klein[8] | Matteo Tonietto[8] | Emily Olafson[9] | Suzanne Baker[10] | Ziad S. Saad[11] | Santiago Bullich[12] | Brian Lopresti[13] | Sandra Sanabria Bohorquez[9] | Mercè Boada[14,15] | Tobey J. Betthauser[16,17,18] | Arnaud Charil[19] | Emily C. Collins[4] | Jessica A. Collins[20] | Nicholas Cullen[2] | Roger N. Gunn[21,22] | Makoto Higuchi[23] | Eric Hostetler[24] | R. Matthew Hutchison[20] | Leonardo Iaccarino[4] | Philip S. Insel[25] | Michael C. Irizarry[16] | Clifford R. Jack Jr[26] | William J. Jagust[27] | Keith A. Johnson[28,29] | Sterling C. Johnson[16,17,18] | Yashmin Karten[2] | Marta Marquié[17,18] | Sulantha Mathotaarachchi[3] | Mark A. Mintun[4] | Rik Ossenkoppele[1,30] | Ioannis Pappas[31,32] | Ronald C. Petersen[33] | Gil D. Rabinovici[34,35] | Pedro Rosa-Neto[36,37] | Christopher G. Schwarz[26] | Ruben Smith[1,38] | Andrew W. Stephens[12] | Alex Whittington[21] | Maria C. Carrillo[39] | Michael J. Pontecorvo[4] | Samantha Budd Haeberlein[3] | Billy Dunn[40] | Hartmuth C. Kolb[3] | Sudhir Sivakumaran[2] | Christopher C. Rowe[6,7,41] | Oskar Hansson[1,42] | Vincent Doré[7,43]

Correspondence
Antoine Leuzy, Clinical Memory Research Unit, Department of Clinical Sciences, Lund University, Sölvegatan 19, 221 84 Lund, Sweden.
Email: antoine.leuzy@med.lu.se

Abstract

INTRODUCTION: Tau-positron emission tomography (PET) outcome data of patients with Alzheimer's disease (AD) cannot currently be meaningfully compared or combined when different tracers are used due to differences in tracer properties, instrumentation, and methods of analysis.

METHODS: Using head-to-head data from five cohorts with tau PET radiotracers designed to target tau deposition in AD, we tested a joint propagation model (JPM) to harmonize quantification (units termed "CenTauR" [CTR]). JPM is a statistical model that simultaneously models the relationships between head-to-head and anchor point

Antoine Leuzy, Lars Lau Raket, Oskar Hansson and Vincent Doré contributed equally.

Funding information: Food and Drug Administration (FDA) of the Department of Health and Human Services (HHS); Swedish Research Council, Grant/Award Number: 2022-00775; ERA PerMed, Grant/Award Number: ERAPERMED2021-184; Knut and Alice Wallenberg foundation, Grant/Award Number: 2017-0383; Strategic Research Area MultiPark; Swedish Alzheimer Foundation, Grant/Award Number: AF-980907; Swedish Brain Foundation, Grant/Award Number: FO2021-0293; The Parkinson foundation of Sweden, Grant/Award Number: 1412/22; Cure Alzheimer's fund; Konung Gustaf V:s och Drottning Victorias Frimurarestiftelse; Skåne University Hospital Foundation, Grant/Award Number: 2020-O000028; Regionalt Forskningsstöd, Grant/Award Number: 2022-1259; ALF agreement, Grant/Award Number: 2022-Projekt0080; NIH/NIA, Grant/Award Numbers: P30-AG062422, U01 AG057195, R35 AG072362; Alzheimer's Association, Grant/Award Number: ZEN-21-848216; American College of Radiology; Rainwater Charitable Foundation; Alliance for Therapeutics in Neurodegeneration

data. JPM was compared to a linear regression approach analogous to the one used in the amyloid PET Centiloid scale.

RESULTS: A strong linear relationship was observed between CTR values across brain regions. Using the JPM approach, CTR estimates were similar to, but more accurate than, those derived using the linear regression approach.

DISCUSSION: Preliminary findings using the JPM support the development and adoption of a universal scale for tau-PET quantification.

KEYWORDS
[18F]Flortaucipir, [18F]RO948, [18F]MK-6240, [18F]GTP1, [18F]PI-2620, Alzheimer's disease, C-Path, CenTauR, Centiloid, CPAD, head-to-head, Imaging, PET, standardization, tau

Highlights

- Tested a novel joint propagation model (JPM) to harmonize quantification of tau PET.
- Units of common scale are termed "CenTauRs".
- Tested a Centiloid-like linear regression approach.
- Using five cohorts with head-to-head tau PET, JPM outperformed linearregression-based approach.
- Strong linear relationship was observed between CenTauRs values across brain regions.

1 | BACKGROUND

Based on both autopsy and in vivo positron emission tomography (PET) studies, tau pathology has been shown to be closely linked to neuronal injury and cognitive decline in Alzheimer's disease (AD).[1–11] Building on the success of amyloid PET,[12,13] the past decade has seen rapid progress in the development of tau-specific PET tracers,[14] including: [18F]flortaucipir ([18F]AV-1451)—approved by the U.S. Food and Drug Administration to aid in the diagnosis of AD[15]—[18F]RO948, [18F]MK-6240, [18F]GTP1, [18F]PI-2620, and [18F]florzolotau ([18F]APN-1607). As a result, tau PET is increasingly used in the clinical research evaluation of patients and as both a predictive and response biomarker in AD clinical trials evaluating disease-modifying therapies.[16] However, the tracers differ in affinity to aggregated tau, have different regional off-target retention, or have not yet been fully characterized[17,18] preventing them from being meaningfully compared or combined. In response to the same challenge for amyloid PET, a harmonization method was developed whereby the outcome of a particular analysis method or tracer could be converted to a common scale,[19] the units of which were termed "Centiloids". The Centiloid method uses an arbitrary scale based on a reference [11C]PIB dataset combined with a prescribed processing methodology and a linear transform that establishes 0 and 100 as the mean values of young Aβ-negative cognitively unimpaired (CU) individuals and typical AD dementia patients, respectively.[19] The Centiloid scale has had a significant impact on AD research, providing a universal scale for amyloid PET and influencing how clinical trials are conducted and reported (e.g., allowing for the combination of multiple amyloid tracers and a common metric for reporting the magnitude of amyloid removal in response to anti-Aβ monoclonal antibody-based therapies).[20–24]

A central limitation of the linear regression-based approach used in developing the Centiloid scale, as it applies to tau PET, however, is the need for a reference tracer. The Centiloid method was built around [11C]PIB due to its high binding affinity, extensive validation, short half-life (enabling two tracer studies in one day) and widespread acceptance as the "gold-standard" at the time of the project. In contrast, there is currently no-established "gold-standard" tau tracer. Further, as there is currently no dataset with head-to-head comparisons between all current tracers, the arbitrary selection of a given ligand as a reference tracer would require the use of intermediate tracers and the subsequent combinations of multiple linear regression equations. Such stepwise mapping between tracers would propagate and amplify noise, which could result in a biased conversion for tracers without direct head-to-head comparison to the reference tracer.

It was against this backdrop that a Working Group of experts across industry and academia led by the Critical Path Institute's (C-Path) Critical Path for Alzheimer's Consortium (CPAD)[25] was convened at the 2022 Alzheimer's Association International Conference to discuss standardization of quantitative tau PET imaging. In addition to exploring the feasibility of adapting the Centiloid method to harmonize tau PET quantification (the units of this scale are termed "CenTauRs" [CTR]),[26] the Working Group developed a joint propagation model (JPM), an approach that does not require the use of a reference tracer. The JPM is based on a statistical model that simultaneously models the

relationships between data from anchor point subjects and data from subjects in multiple head-to-head studies and the CTR scale, providing mapping equations for multiple tracers. In this report, we describe the JPM for the standardization of tau PET imaging and present CTR values derived using this approach across five cohorts with head-to-head tau PET. As a validation step, we compared CTR values from this approach to those from a reference-based linear regression approach similar to that used for the Centiloid derivation and demonstrate how the JPM offers a more straightforward approach to tau PET harmonization. Further, we illustrate that the mapping equations from individual tracer standardized uptake value ratios (SUVRs) to the CTR scale are more accurately estimated by the JPM compared to the linear regression approach. Importantly, the approach outlined here is not meant to serve as a definitive method for converting tau PET outcome data to CTRs, but rather to serve as a starting point for approaching the standardization of tau PET that subsequent efforts can expand upon.

RESEARCH IN CONTEXT

1. **Systematic review**: The authors used PubMed to search for articles dealing with the standardization of quantitative tau positron emission tomography (PET) imaging.
2. **Interpretation**: A strong linear relationship was observed between CenTauR (CTR) values across brain regions. Using the joint propagation model (JPM) approach, CTR estimates were similar to, but more accurate than, those derived using the linear regression approach.
3. **Future directions**: Further studies are required to test the JPM in large samples of individuals spanning the Alzheimer's disease (AD) clinical continuum.

2 | METHODS

2.1 | Head-to-head datasets

A total of 119 individuals with head-to-head tau PET were included from five cohorts: [^{18}F]RO948 vs [^{18}F]flortaucipir (BioFINDER-2, n = 37),[27] [^{18}F]MK-6240 vs [^{18}F]flortaucipir (University of Pittsburgh, n = 15),[28] [^{18}F]GTP1 vs [^{18}F]PI-2620 (Roche/Invicro, n = 27), [^{18}F]GTP1 vs [^{18}F]MK-6240 (Roche/Invicro, n = 22), and [^{18}F]RO948 vs [^{18}F]PI-2620 (Fundació ACE Healthy Brain Initiative (FACEHBI) study, n = 18).[29] Anchor point values (see Section 2.2) were derived from an additional 327 individuals: [^{18}F]flortaucipir (BioFINDER and Avid A05, n = 54); [^{18}F]GTP1 (Roche/Invicro, n = 26); [^{18}F]MK-6240 (AIBL, n = 164); [^{18}F]PI-2620 (LMI, n = 19); and [^{18}F]RO948 (BioFINDER-2, n = 64).

2.2 | Anchor point datasets

Like the Centiloid method, the CTR process uses a scale that is anchored at 0 (CTR-0) and 100 (CTR-100). Criteria for the CTR-0 group were CU individuals who were negative on both amyloid (visual read and Centiloids < 10, a cutoff associated with the absence of Aβ plaques[20,30]) and tau PET (visual read). Criteria for the CTR-100 group were having a clinical diagnosis of AD dementia,[31] age < 75, Mini-Mental State Examination (MMSE) > 20 and being positive on both amyloid (visual read and Centiloids > 50) and tau PET (visual read). Although visual assessment methods are available for the tau tracers included here,[32–36] due to differences between them, we defined tau PET positivity on visual read for all tracers as substantial bilateral temporal (including the mesial temporal lobes) and parietal uptake (see Supplementary Figure 1), a retention pattern consistent with the neuropathological distribution of tau in Braak stage ≥ IV in AD.[37,38] In the BioFINDER-2 cohort—used to set anchor points for [^{18}F]RO948—Aβ-positivity among AD dementia cases was established using CSF Aβ42/Aβ40. This is unlikely to have biased group assignment given the high concordance between CSF Aβ42/Aβ40 and amyloid PET.[39] The age cap of 75 was intentional because older subjects have much lower tau PET SUVR values;[40,41] anchoring on younger AD patients ensured that we covered the full range of SUVR values and did not have anchor populations composed of different proportions of younger and older subjects. A cutoff of 20 on the MMSE was chosen to exclude cases with widespread atrophy that could reduce the tau PET signal. 50 Centiloids was chosen as this has previously been shown to be the point where a significant rise in the prevalence of cortical tau occurs in AD.[42,43]

Applying the anchor point criteria to different datasets available to the Working Group resulted in the following groups: [^{18}F]flortaucipir (n = 29 CTR-0, n = 25 CTR-100 [BioFINDER, Avid A05]); [^{18}F]RO948 (n = 36 CTR-0, n = 36 CTR-100 [BioFINDER-2]); [^{18}F]MK-6240 (n = 120 CTR-0, n = 32 CTR-100 [AIBL]); [^{18}F]GTP1 (n = 7 CTR-0, n = 19 CTR-100 [Roche/Invicro]); [^{18}F]PI-2620 (n = 10 CTR-0, n = 9 CTR-100 [Life Molecular Imaging]). A sensitivity analysis using young (age < 40 years) Aβ-negative CU individuals to define the CTR-0 values was also performed (see Supplementary Figure 2).

2.3 | PET imaging and analysis

Tau PET data were acquired on different platforms using different acquisition windows (for complete details, see Supplementary Methods 1): [^{18}F]PI-2620 (45-75 min), [^{18}F]GTP1 (60-90 min), [^{18}F]RO948 (70-90 min), [^{18}F]flortaucipir (80-100 min), and [^{18}F]MK-6240 (70-90 min [University of Pittsburgh] or 90-110 min [Roche/Invicro and AIBL]). SUVR images were created using the inferior cerebellar cortex as the reference region.[44] All individuals from these different studies also underwent a T1-weighted MRI.

2.4 | Standard regions of interest

Recently, a "universal" tau PET region of interest (ROI) was derived based on the areas showing differences in signal between AD dementia

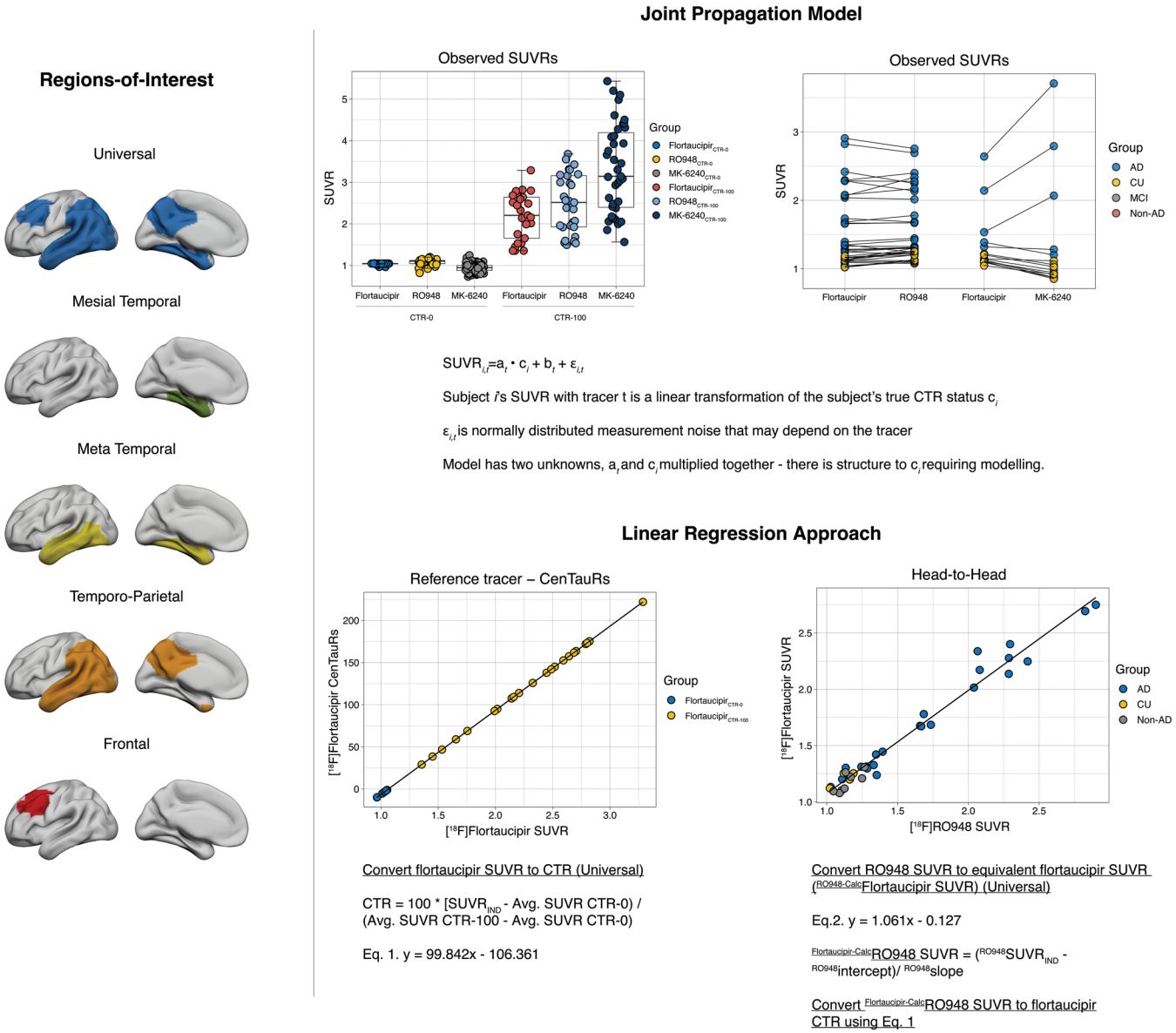

FIGURE 1 Overview of the CenTauR ROIs, the JPM and the linear regression approach. Universal and subregion regions of interest (ROIs) (left) along with an overview of both the joint propagation model (JPM) and the linear regression approaches (right). Using the JPM (top right), we assume that CenTauR (CTR) is common latent scale that has given rise to the observed data, and we do not assume a reference tracer. Using both anchor point (left) and head-to-head (right) data, maximum likelihood estimation is used to estimate the parameters that are most likely to generate the observed data. From these estimated parameters, equations that map standardized uptake value ratio (SUVR) values to CTRs can then be generated for a given tracer. Using the linear regression approach (bottom right; here assuming [^{18}F]flortaucipir as the reference tracer), we first derive the equation to convert [^{18}F]flortaucipir SUVR to (Equation 1) using anchor point values (left). Next, [^{18}F]RO948 SUVR are converted to their equivalent in [^{18}F]flortaucipir (i.e., Flortaucipir-Calc) (Equation 2). Using Equation 1, these Flortaucipir–Calc values can then be converted to CTRs. [^{18}F]Flortaucipir was used as the reference tracer as it is currently the most widely available and most widely studied tau tracer, and the only one validated against autopsy cases and approved by U.S. Food and Drug Administration.

patients and Aβ-negative CU individuals that were common across six different tracers ([^{18}F]flortaucipir, [^{18}F]RO948, [^{18}F]MK-6240, [^{18}F]GTP1, [^{18}F]PI-2620, and [^{18}F]PM-PBB3) (Figure 1; for complete details, see Supplementary Methods 2).[26] To cover the full spectrum of tau aggregation from early to later affected areas, four additional ROIs were defined within the constraints of the universal mask: mesial temporal, meta temporal, temporo-parietal, and frontal. These ROIs have been made available on the publicly accessible Global Alzheimer's Association Information Network (GAAIN; http://www.gaain.org/Centaur) website.

2.5 | The JPM

We developed the JPM as an approach for harmonizing tau PET data without the need for a reference tracer. This approach further allows

incorporation of anchor point data from multiple tracers and models the random variation (i.e., noise) in all tracers. This is in contrast to simple linear regression approaches which apply an asymmetric assumption to map head-to-head data against a reference tracer. The JPM is a nonlinear mixed-effects model that may seem complex compared to a set of linear regressions, however, the result of the JPM will be a set of linear mapping equations that map tracer SUVRs to CTRs. Therefore, there will be no increased complexity for end users. The JPM is based on the basic assumption that SUVRs are noisy tracer-specific linear transformations of the true CTR value of the subject being measured. Thus, the JPM poses the problem of calculating regional CTR values for a subject as an inverse problem where we are inferring the CTR value that was most likely to produce the observed SUVR. In its most general form, the JPM models the regional SUVR of subject i with tracer t as

$$SUVR_{it} = f_t(c_i) + \varepsilon_{it} \tag{1}$$

where f_t is the tracer-specific linear mapping of the subject's underlying CTR value c_i to the SUVR scale and ε_{it} is a term representing measurement noise of tracer t. Conditional on c_i, Equation (1) looks structurally like a simple nonlinear regression model, but since c_i is not known, one cannot estimate relationships between tracers and the CTR scale without additional assumptions.

In this work, we propose a model based on the following assumptions: (1) the relation between CTR and SUVR is linear $f_t(c_i) = a_t \cdot c_i + b_t$; (2) for subjects meeting the CTR-0 anchor point criterion, CTR c_i are modeled as a random effect, assumed to be normally distributed around 0 with an unknown variance, $c_i \sim N(0, \sigma_0^2)$; (3) for subjects meeting the CTR-100 anchor point criterion, CTRs c_i are modeled as a random effect, assumed to be normally distributed around 100 with unknown variance, $c_i \sim N(100, \sigma_{100}^2)$; (4) for subjects with head-to-head data, CTRs c_i are modeled as a fixed effect assumed to be identical across tracers; (5) the noise term is assumed to be zero-mean normally distributed $\varepsilon_{it} \sim N(0, \sigma_t^2)$ with a structured variance that assumes that all tracers have identical variance σ^2 on the CTR scale, meaning that the SUVR scale variance is given by $\sigma_t^2 = a_t^2 \cdot \sigma^2$. Based on the above assumptions, the model can be written out as

$$\begin{gathered} SUVR_{it} = a_t \cdot (1_{\mathrm{H2H}(i)} \cdot c_i + 1_{\mathrm{CTR-0}(i)} \cdot c_i^0 + 1_{\mathrm{CTR-100}(i)} \cdot c_i^{100}) + b_t + \varepsilon_i t \\ a_t, b_t, c_i \in \mathbb{R} \\ c_i^0 \sim N(0, \sigma_0^2) \\ c_i^{100} \sim N(100, \sigma_{100}^2) \\ \varepsilon_{it} \sim N(0, a_t^2 \cdot \sigma^2) \end{gathered} \tag{2}$$

where $1_{\mathrm{H2H}(i)}$ is the indicator function that is 1 when subject i is in the head-to-head cohort and 0 otherwise, and similarly with $1_{\mathrm{CTR-0}(i)}$ and $1_{\mathrm{CTR-100}(i)}$ for the CTR-0 and 100 anchor point cohorts. By specifying all relationships in a single joint model, the JPM is capable of propagating information between all tracers through anchor point data and multiple head-to-head studies.

Based on maximum likelihood estimates $\hat{a}_t$ and $\hat{b}_t$ from model (2), CTRs can be predicted based on a simple linear transformation of SUVR values

$$\hat{c}_i = 1/\hat{a}_t \cdot (SUVR_{it} - \hat{b}_t).$$

The model (2) assumes different variances in the measurement error term across tracers, but structured in such a way that the signal-to-noise ratio is identical across tracers on the CTR scale. This assumption was motivated by lack of structured data (e.g., test-retest data from individual tracers) in the presently used datasets that could enable simultaneous estimation of mapping equations to the CTR scale and individual tracer-specific variance parameters. A custom C++ implementation of the models was developed using the Template Model Builder framework[45] and fitted in R using maximum likelihood estimation. The implementation is publicly available on GitHub: https://github.com/larslau/JPM.

2.6 | Linear regression approach

The Centiloid method for amyloid PET harmonization was based on estimating a linear mapping of SUVR values for a given tracer to SUVR values obtained using [^{11}C]PIB, which served as the reference tracer.[19] Anchor points defining 0 and 100 on the Centiloid scale were estimated using Aβ-negative CU individuals and typical AD dementia patients, respectively, enabling linear mapping of reference tracer SUVR to the harmonized scale. Calibration of other tracers to the harmonized scale is possible using head-to-head data, based on a simple linear regression with reference tracer SUVR as the dependent variable and the nonreference tracer SUVR as the independent variable. Using the linear regression estimates, the nonreference tracer SUVR can be mapped to the reference tracer SUVR, which can in turn be mapped to the Centiloid scale. The process of converting SUVR values to CTRs using this approach is illustrated in Figure 1.

2.7 | Statistical analysis

All analyses were performed in R, version 4.2.1 (R Foundation). The association between CTR values from the linear regression approach and the JPM, as well as between JPM-based CTR values in head-to-head cohorts, was assessed across ROIs using coefficient-of-determination (R^2).

Unlike the JPM, the linear regression approach requires the choice of a reference tracer. Even with a single set of head-to-head data including two tracers, the mapping from each tracer to the other using the linear regression approach would not lead to fully symmetric mappings. To investigate the impact of the choice of reference tracer and potential multistep mappings through tracers in head-to-head studies, we estimated the mapping of every tracer to every other tracer (one or two steps) and evaluated the bias associated with mapping one tracer

TABLE 1 Characteristics of head-to-head participants

	Diagnostic groups			
Parameter	**CU**	**MCI**	**AD**	**Non-AD**
Cohort 1: [^{18}F]RO948 *vs* [^{18}F]flortaucipir				
N	5	–	24	8
Age (y)	77.5 ± 6.4	–	74.2 ± 7.1	72.75 ± 6.54
Sex (M/F)	3/3	–	11/13	3/5
MMSE	29.31 ± 0.69	–	23.20 ± 2.82	25.47 ± 3.75
Amyloid positive, n (%)	2 (40%)	–	24 (100%)	2 (25%)
Cohort 2: [^{18}F]MK-6240 *vs* [^{18}F]flortaucipir				
N	9	1	5	–
Age (y)	76.44 ± 3.88	77	70.80 ± 13.70	–
Sex (M/F)	1/8	1/0	1/4	–
MMSE	28.22 ± 3.07	22	19.20 ± 7.63	–
Amyloid positive, n (%)	5 (56%)	1 (100%)	5 (100%)	–
Cohort 3: [^{18}F]GTP1 *vs* [^{18}F]PI-2620				
N	5	10	12	–
Age (y)	71 ± 1.0	72 ± 5.4	74 ± 3.0	–
Sex (M/F)	4/1	4/6	7/5	–
MMSE	30.0 ± 0.0	26.9 ± 1.8	22.5 ± 4.4	–
Amyloid positive, n (%)	0 (0%)	10 (100%)	12 (100%)	–
Cohort 4: [^{18}F]GTP1 *vs* [^{18}F]MK-6240				
N	5	3	14	–
Age (y)	68.0 ± 2.5	73.7 ± 4.0	71.6 ± 7.9	–
Sex (M/F)	1/4	1/2	7/7	–
MMSE	29.8 ± 0.4	27.6 ± 1.1	17.9 ± 4.0	–
Amyloid positive, n (%)	1 (20%)	3 (100%)	14 (100%)	–
Cohort 5: [^{18}F]RO948 *vs* [^{18}F]PI-2620				
N	13	5	–	–
Age (y)	73 ± 7	77 ± 3	–	–
Sex (M/F)	7/6	2/3	–	–
MMSE	29.62 ± 0.65	28.20 ± 1.30	–	–
Amyloid positive, n (%)	7 (54%)	2 (40%)	–	–

Abbreviations: AD, Alzheimer's disease; CU, cognitively unimpaired; MCI, mild cognitive impairment; MMSE, Mini-Mental State Examination.

to another tracer and back to the original tracer using the estimated mapping equations. The bias was calculated as percent deviation in mean SUVR of the CTR-0 and CTR-100 anchor point values scanned with the original tracer.

To compare the performance of the JPM and the linear regression approach, 20 replications of five-fold cross-validation analysis (100 evaluations) were performed. For the linear regression approach, where a reference tracer is required, we chose [^{18}F]flortaucipir (i.e., [^{18}F]flortaucipir data to set the anchor points and [^{18}F]flortaucipir/[^{18}F]MK-6240 and [^{18}F]flortaucipir/[^{18}F]RO948 head-to-head studies for the analysis). In each cross-validation study, SUVR values from the universal ROI from participants from the [^{18}F]flortaucipir/[^{18}F]MK-6240 and [^{18}F]flortaucipir/[^{18}F]RO948 head-to-head cohorts were split into five equally sized folds. Each fold was then held out as a test set while the linear regression approach and the JPM were fitted using data from the remaining four folds. Performance of the methods was evaluated on the held-out head-to-head data by (1) mapping the [^{18}F]flortaucipir SUVRs from both head-to-head datasets to the CTR scale using the estimated parameters and calculating the mean square error; and (2) mapping [^{18}F]MK-6240 and [^{18}F]RO948 SUVR values to [^{18}F]flortaucipir SUVR values using the estimated parameters and calculating the mean square error. While the linear regression approach only used [^{18}F]flortaucipir anchor point data, the JPM used all available anchor point data.

To quantify the impact of the difference in available anchor point data, a sensitivity analysis was done with the JPM using only

TABLE 2 Characteristics of anchor point participants.

Tracer	Anchor group	N	Age (y)	Sex (M/F)	MMSE	Amyloid PET, Centiloids	Amyloid PET, Pos. visual read	Tau PET, Pos. visual read
[^{18}F]RO948	CTR-0	36 (CU)	72.29 ± 5.94	16/20	28.78 ± 1.23	−11.17 ± 5.30	0 (0%)	0 (0%)
	CTR-100	36 (AD)	62.45 ± 3.80	21/15	24.40 ± 2.18	72.87 ± 14.90	36 (100%)*	36 (100%)
[^{18}F]Flortaucipir	CTR-0	29 (CU)	68.04 ± 10.41	16/13	28.51 ± 0.59	−6.50 ± 7.87	0 (0%)	0 (0%)
	CTR-100	25 (AD)	61.94 ± 4.39	9/16	23.12 ± 1.69	67.49 ± 17.32	25 (100%)	25 (100%)
[^{18}F]MK-6240	CTR-0	120 (CU)	67.26 ± 6.70	57/63	29.0 ± 1.1	−15.47 ± 5.10	0 (0%)	0 (0%)
	CTR-100	32 (AD)	64.49 ± 6.35	17/14	24.0 ± 1.9	62.47 ± 11.70	32 (100%)	32 (100%)
[^{18}F]GTP1	CTR-0	15 (CU)	64 ± 6.91	8/7	29.5 ± 0.83	0.25 ± 10.99	0 (0%)	0 (0%)
	CTR-100	25 (AD)	67 ± 5.88	13/12	23.3 ± 2.11	98.27 ± 27.04	25 (100%)	25 (100%)
[^{18}F]PI-2620	CTR-0	10 (CU)	59.20 ± 7.83	6/4	29 ± 1.25	−2.06 ± 6.06	0 (0%)	0 (0%)
	CTR-100	9 (AD)	65.11 ± 8.78	4/5	18.78 ± 6.80	105.31 ± 18.64	9 (100%)	9 (100%)

Note: In BioFINDER-2, Aβ-positivity among AD dementia cases was established using CSF Aβ42/Aβ40.
Abbreviations: AD, Alzheimer's disease; CTR, CenTauR; CU, cognitively unimpaired; MMSE, Mini-Mental State Examination; PET, positron emission tomography; Pos., positive.

[^{18}F]flortaucipir anchor point data. Mean square prediction errors on the test sets were compared using the paired Wilcoxon rank sum test. Last, the estimated internal relationships between tracers from the JPM were compared to the regression estimates from head-to-head studies and robustness to potential biases in selected anchor-point cases was evaluated by comparing the JPM-derived SUVR-to-SUVR mapping equations between tracers using: (1) all data; (2) only [^{18}F]flortaucipir anchor point data; and (3) by artificially biasing [^{18}F]MK-6240 anchor point values by 30%. For the third sensitivity analysis, [^{18}F]MK-6240 and 30% were chosen due to [^{18}F]MK-6240 being the tracer with the largest anchor point groups (i.e., where bias would potentially have the greatest effect) and 30% representing a high degree of bias.

3 | RESULTS

Participant characteristics for the head-to-head and anchor point cohorts are summarized in Tables 1 and 2. The five CTR ROIs, as well as an overview of both the JPM and linear regression approaches, are shown in Figure 1. JPM-based CTR values for head-to-head and anchor point cohorts are shown in Figure 2. Using head-to-head data, strong linear associations (R^2) were observed between tracers across all ROIs (Figure 3): [^{18}F]RO948 vs [^{18}F]flortaucipir, average 0.977 (range 0.959 [frontal] to 0.986 [universal]); [^{18}F]MK-6240 vs [^{18}F]flortaucipir, average 0.985 (range 0.976 [mesial temporal] to 0.991 [frontal]); [^{18}F]GTP1 vs [^{18}F]MK-6240, average 0.928 (range 0.904 [frontal] to 0.945 [meta temporal]); [^{18}F]GTP1 vs [^{18}F]PI-2620, average 0.945 (range 0.919 [mesial temporal] to 0.954 [meta temporal]); [^{18}F]RO948 vs [^{18}F]PI-2620, average 0.903 (range 0.762 [frontal] to 0.958 [meta temporal]). Because both harmonization methods were based on linear transformations, R^2 values were identical to the SUVR findings on the CTR for the linear regression and JPM approaches, although the range of CTR values differed. This difference is due to an assumption inherent to many linear regression models, namely that the response variable is subject to error but that the predictor variable is not,[46] resulting in slightly different solutions depending on the choice of predictor variable (i.e., reference tracer).

The JPM provides simultaneous estimates of mapping equations to the CTR scale for all tracers. These estimates provide a consistent and symmetric way of mapping each tracer SUVR to every other tracer SUVR by first using the estimated mapping equation to CTR, and then applying the inverse mapping equation to another tracer SUVR. However, the mapping equations estimated by the linear regression approach with different choices of reference tracer are asymmetric. As reported in Table 3, this asymmetry results in deviation from identity when mapping tracer SUVRs forward and then backwards between two tracers. Using the current datasets, these deviations are exacerbated by multistep mappings using an intermediate tracer (e.g., from [^{18}F]RO948 over [^{18}F]PI-2620 to [^{18}F]GTP1 and back again). Across the additional sensitivity analyses performed for the JPM (i.e., using only [^{18}F]flortaucipir anchor points and artificially biasing [^{18}F]MK-6240 anchor point values by 30%), there was little impact on the estimated SUVR-to-SUVR equations (Figure 4).

Across 20 replications of five-fold cross-validation (totaling 100 evaluations) comparing the linear regression approach with JPM on the CTR scale, the JPM consistently resulted in lower mean square prediction error (mean 45.0 vs. 76.8). This was primarily an effect of a slightly more compressed range of the CTR scale for the JPM compared to the linear regression approach (Figure 5). The difference in the CTR scale between the two methods was much less when only using [^{18}F]flortaucipir anchor point data (Supplementary Figure 3). When mapping results back to the [^{18}F]flortaucipir scale, results were very similar in terms of mean square prediction error (mean JPM 0.00742, linear regression 0.00874; $p = 0.2114$) (Figure 5). In six evaluations, the linear regression approach produced mean square prediction errors that were more than double those of JPM. The lower prediction error of the JPM in these cases was the result of JPM being able to propagate

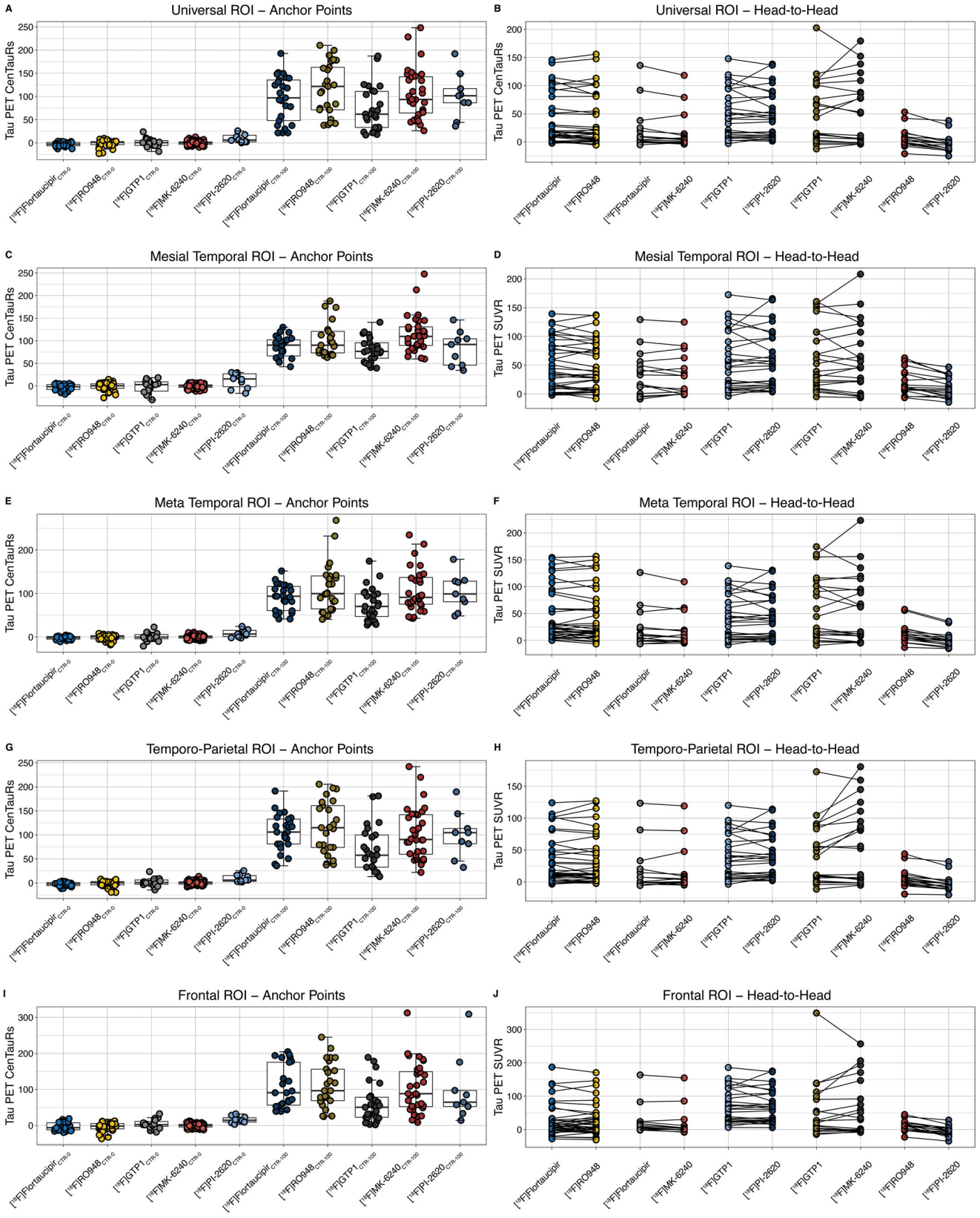

FIGURE 2 CenTauR (CTR) values across regions of interest in anchor point and head-to-head cohorts. CTR values are shown for anchor point subjects on the left and for head-to-head subjects on the right for each ROI: universal (A, B), mesial temporal (C, D), meta temporal (E, F), temporoparietal (G, H), and frontal (I, J).

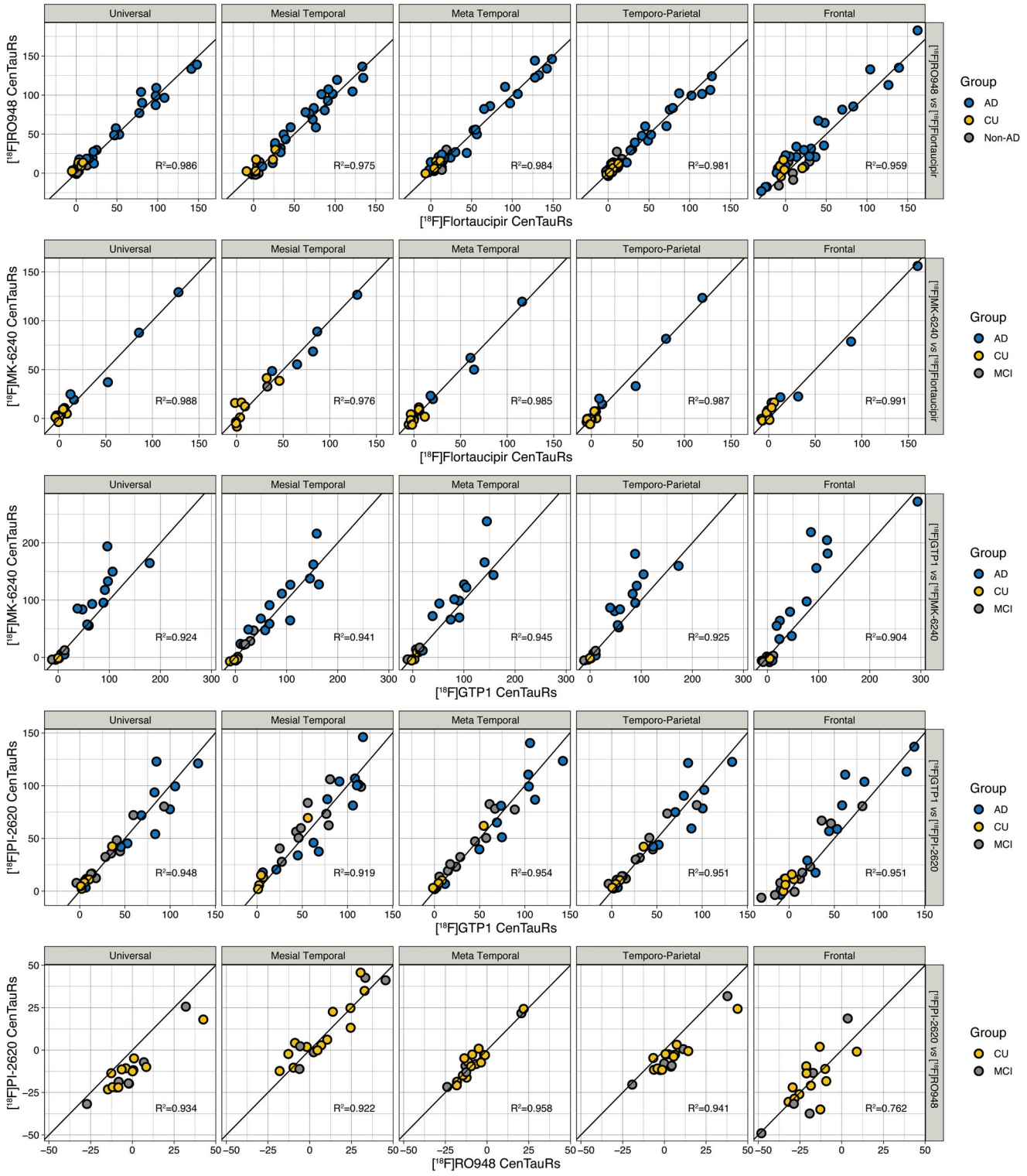

FIGURE 3 Associations between joint propagation model (JPM)-based CenTauR (CTR) values across head-to-head cohorts and regions of interest (ROIs) (each row, left to right: universal, mesial temporal, meta temporal, temporoparietal, and frontal) for head-to-head cohorts. Top row, [18F]RO948 vs [18F]flortaucipir; second row, [18F]MK-6240 vs [18F]flortaucipir; third row, [18F]GTP1 vs [18F]MK-6240; fourth row, [18F]GTP1 vs [18F]PI-2620; bottom row, [18F]RO948 vs [18F]PI-2620.

TABLE 3 Multistep mapping using the linear regression approach

			Mean SUVR in starting-tracer anchor point subjects		Back-and-forth SUVR mapping deviation	
Starting tracer	Intermediate tracer	Target tracer	CTR-0	CTR-100	CTR-0	CTR-100
[^{18}F]Flortaucipir	—	[^{18}F]MK-6240	1.06	2.13	1%	−1%
[^{18}F]Flortaucipir	[^{18}F]MK-6240	[^{18}F]GTP1	1.06	2.13	2%	−2%
[^{18}F]Flortaucipir	—	[^{18}F]RO948	1.06	2.13	1%	−1%
[^{18}F]Flortaucipir	[^{18}F]RO948	[^{18}F]PI-2620	1.06	2.13	5%	−11%
[^{18}F]GTP1	—	[^{18}F]MK-6240	1.08	1.69	1%	0%
[^{18}F]GTP1	[^{18}F]MK-6240	[^{18}F]Flortaucipir	1.08	1.69	2%	−1%
[^{18}F]GTP1	—	[^{18}F]PI-2620	1.08	1.69	4%	−1%
[^{18}F]GTP1	[^{18}F]PI-2620	[^{18}F]RO948	1.08	1.69	3%	−10%
[^{18}F]MK-6240	—	[^{18}F]Flortaucipir	0.93	3.30	1%	−1%
[^{18}F]MK-6240	[^{18}F]Flortaucipir	[^{18}F]RO948	0.93	3.30	4%	−3%
[^{18}F]MK-6240	—	[^{18}F]GTP1	0.93	3.30	3%	−2%
[^{18}F]MK-6240	[^{18}F]GTP1	[^{18}F]PI-2620	0.93	3.30	13%	−6%
[^{18}F]PI-2620	—	[^{18}F]GTP1	1.17	2.12	4%	−2%
[^{18}F]PI-2620	[^{18}F]GTP1	[^{18}F]MK-6240	1.17	2.12	5%	−3%
[^{18}F]PI-2620	—	[^{18}F]RO948	1.17	2.12	−2%	−12%
[^{18}F]PI-2620	[^{18}F]RO948	[^{18}F]Flortaucipir	1.17	2.12	−2%	−13%
[^{18}F]RO948	—	[^{18}F]Flortaucipir	1.03	2.40	1%	−1%
[^{18}F]RO948	[^{18}F]Flortaucipir	[^{18}F]MK-6240	1.03	2.40	2%	−2%
[^{18}F]RO948	—	[^{18}F]PI-2620	1.03	2.40	3%	−12%
[^{18}F]RO948	[^{18}F]PI-2620	[^{18}F]GTP1	1.03	2.40	8%	−15%

Note: Intermediate tracer is the tracer that allowed for mapping SUVR values from the given start tracer to the target tracer in a maximum of two steps. Abbreviation: SUVR, standardized uptake value ratio. CTR, CenTauR; CTR-0, CTR-0 anchor point group; CTR-100, CTR-100 anchor point group.

information from both anchor-point data and across tracers, minimizing the effect of nonrepresentative data. When removing anchor point data from [^{18}F]RO948 and [^{18}F]MK-6240, the prediction error in these six cases was still substantially reduced using the JPM compared to the linear regression approach (Supplementary Figure 3).

4 | DISCUSSION

The JPM-based analysis is based on two assumptions that will require further evaluation. First, we assumed that the relationship between SUVR and CTRs could be modeled as a linear function. While there was no indication of nonlinearity based on the included head-to-head studies, we had relatively few high tau cases with SUVR values in the range where deviations from linearity may occur. The JPM does allow for nonlinear relationships, however, by using a parametric nonlinear function, such as a sigmoid function, in Equation (1) instead of the chosen linear function. The second assumption was that all tracers had the same signal-to-noise ratio on the CTR scale, because the current data did not allow for a fully data-driven estimation of tracer-specific variance parameters. Although this may not be the case, we determined that this assumption was the most unbiased assumption pending the availability of robust test-retest data. In this analysis, tau PET test-retest data was not available for all tracers used, rendering the variance parameters at tracer level unidentifiable. Though the impact of this assumption on the mapping equations is likely limited, future analyses are required to address the impact of different signal-to-noise ratios, including the possibility of using this parameter to weight tracers. This may be especially important in the context of sample size calculations for longitudinal studies of disease progression or treatment response.

The current study took advantage of a recently proposed universal tau ROI.[26] Derived from common brain areas showing high signal in Aβ-positive AD patients across the five tracers included here, the universal ROI minimizes signal dilution and provides a mask that can be used across tau tracers. Moreover, the delineation of subregions also allows for the examination of specific brain regions separately given that they behave differently over time: tau accumulation in the mesial temporal lobe, for instance, occurs early followed by a plateau, while the temporoparietal cortex appears to be the most sensitive region to capture tau accumulation over time and is likely large enough to provide robust estimates of changes in tau burden in a clinical trial.[47,48] This approach

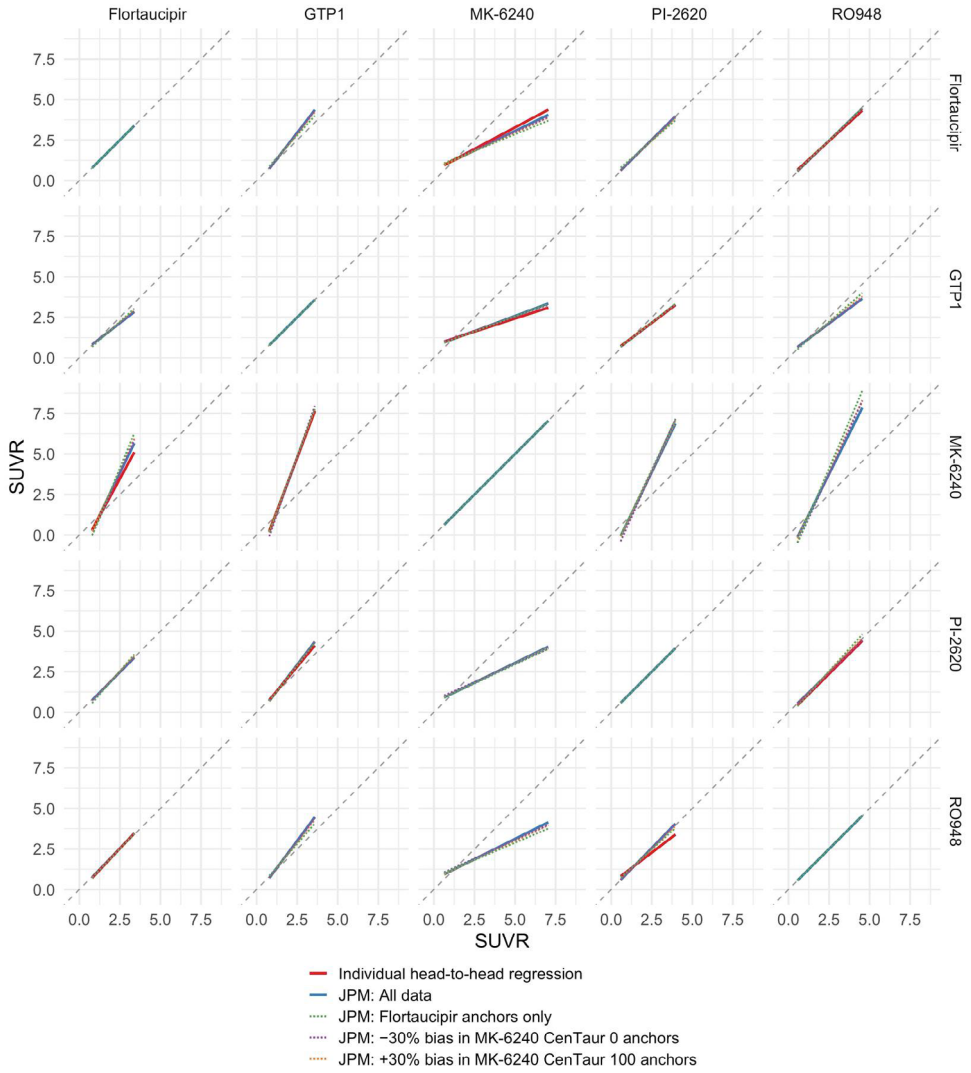

FIGURE 4 Sensitivity analyses varying anchor point values using the joint propagation model (JPM). Comparison of tracer-to-tracer standardized uptake value ratio (SUVR) mapping equations from head-to-head cohorts are shown in solid red, with results from JPM based equations shown in solid blue. Dashed lines show sensitivity analyses using only [^{18}F]flortaucipir anchor point data (green) and when varying [^{18}F]MK-6240 anchor point data by 30% (CenTauR: CTR-0, purple; CTR-100, orange). High agreement was observed between JPM results and head-to-head equations generated by linear regression in each of the five head-to-head cohorts. The biggest deviation was observed for [^{18}F]PI-2620 vs [^{18}F]RO948, where head-to-head data was limited in its SUVR range. Across all three sensitivity analyses, there was very little impact on the estimated SUVR-to-SUVR equations. [^{18}F]Flortaucipir was used as the reference tracer as it is currently the most widely available and most widely studied tau tracer, and the only one validated against autopsy cases and approved by U.S. Food and Drug Administration.[34]

was designed to capture both the overall burden and distribution of tau in the brain as well as tau progression and heterogeneous patterns of tau distribution due to primary age-related tauopathy and tau subtypes.[49,50]

In addition to the need for a reference tracer, the linear regression approach is limited by the fact that it does not incorporate nonreference tracer anchor point data. Additional limitations include: (1) the lack of symmetric solutions using linear regression; (2) no clear way to include head-to-head studies that do not include the reference tracer; and (3) increasing complexity based on the number of head-to-head comparisons due to its stepwise approach. The JPM, by contrast, is not subject to these limitations and performs the conversion to CTRs in a single step, where all parameters are estimated using the full data set (i.e., head-to-head and anchor point data). Future studies may also wish to harmonize additional tau PET tracers. The JPM allows for this either by refitting the models after inclusion of the new data or by fixing the existing mapping equations and then estimating equations for the new tracer(s) using only head-to-head or anchor point data.

A strength of this study is the inclusion of data from all currently available cross-sectional tau PET head-to-head cohorts. Further, analyses were performed using cortical ROIs based on the areas showing a difference between Aβ-positive AD dementia cases and Aβ-negative CU individuals using tau PET data from the five tracers included here.

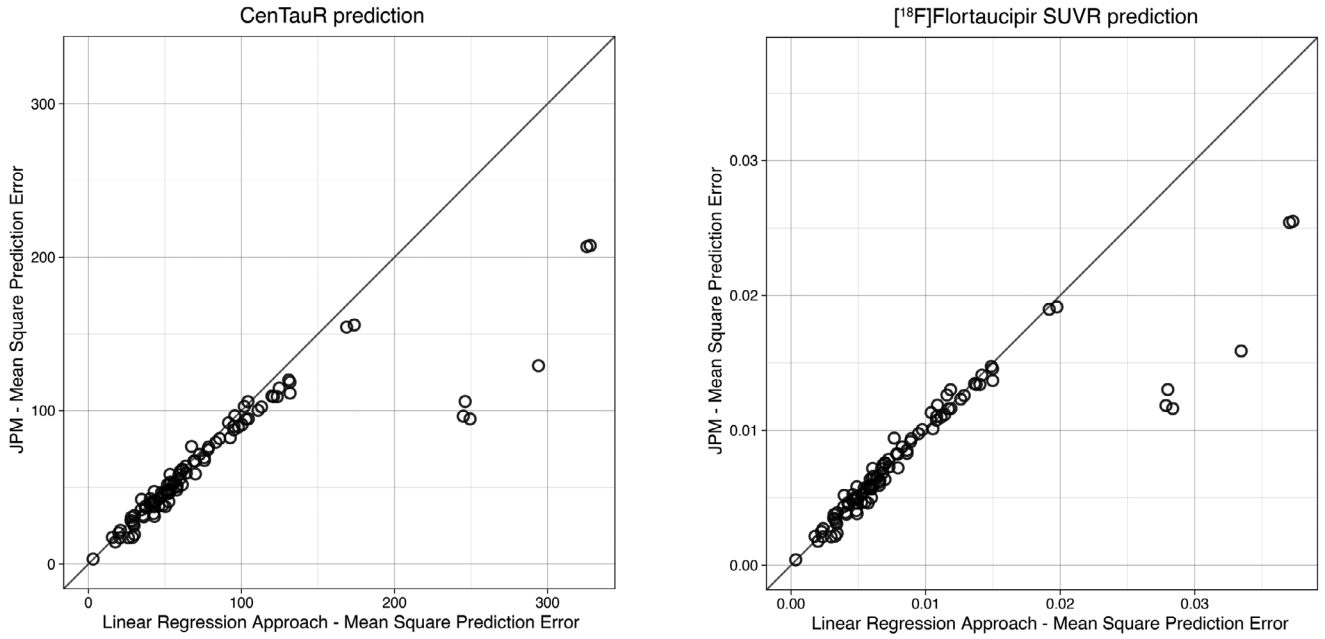

FIGURE 5 Mean square prediction error of the linear regression approach and the joint propagation model (JPM) on the CenTauR (CTR) scale and on the [^{18}F]flortaucipir standardized uptake value ratio (SUVR) scale across 20 replications of five-fold cross-validation. Across 20 replications of five-fold cross validation (totaling 100 evaluations), comparing the linear regression method with JPM on the CTR scale (left), the JPM consistently resulted in lower mean square prediction error (mean 45.0 vs. 76.8). This was primarily an effect of a slightly more compressed range of the CTR scale for the JPM compared to the linear regression method. When mapping results to [^{18}F]flortaucipir SUVR values (right), similar results were observed in terms of mean square prediction error (mean JPM 0.00742, linear regression approach 0.00874). [^{18}F]Flortaucipir was included in the sensitivity analyses as it is currently the most widely available and most widely studied tau tracer, and the only one validated against autopsy cases and approved by U.S. Food and Drug Administration.[34]

These ROIs included both the common global "universal" region as well as subregions to assess the progression of tau aggregation from early to later affected areas. Limitations include the modest number of head-to-head cases, the overall limited range of tau PET severity and the fact that in certain cohorts (i.e., [^{18}F]GTP1 and [^{18}F]flortaucipir vs. [^{18}F]MK-6240), only a handful of cases showed elevated tracer retention. Further, head-to-head data was not available for several other tau PET tracers, including [^{18}F]florzolotau and [^{18}F]JNJ311. Though SUVR values were generated using the same inferior cerebellar cortex ROI as the reference region, which is widely used to avoid the frequently seen signal in the head of the cerebellar vermis as well as spill-over from the occipital lobe—this part of the cerebellum can be affected by partial-volume effects and problems associated with proximity to the edge of the field of view.[51] Attempts to define a universal cerebellar tau mask are already underway[52] and will need to be incorporated into subsequent iterations of this harmonization work. In addition, though concordance between CSF Aβ42/Aβ40 and amyloid PET in AD dementia is high, it is not perfect;[39,53] as such, we cannot rule out that some of the AD dementia cases include in the CTR-100 group for [^{18}F]RO948 may have had Centiloid values below 50. Given the positive association between amyloid and tau PET in AD dementia,[43] this could have resulted in lower values overall for the CTR-100 group. Last, due to differences in kinetics, the tracers included here may not reach transient equilibrium over the course of their acquisition windows. As a result, SUVR estimates will be biased as a function of scan time, brain region and underlying tau burden.[54] This problem cannot be accounted for using the JPM. Recent work, however, suggests that this can be corrected for using a one-step nonlinear algebraic transform of SUVR values that is a function of radiotracer-dependent parameters.[55,56]

In summary, the preliminary findings presented here using the JPM support the idea of a standardized scale for tau PET. Subsequent work will address (1) the impact of different signal-to-noise ratios across tracers on mapping equations, with tracer-specific variance parameters derived from test-retest data and longitudinal data on nonprogressors; (2) the implementation of the JPM in additional larger datasets, including those from early-onset AD, which shows a higher burden of tau tangles and a different regional distribution of tau pathology compared to late-onset AD;[57] (3) compare the JPM with other methods, including approaches that are currently being developed in the Head-to-Head Harmonization of Tau Tracers in Alzheimer's Disease (HEAD) study.[58] In this multisite trial, [^{18}F]flortaucipir and [^{18}F]MK-6240 will be compared head-to-head at baseline and longitudinally in approximately 600 individuals across the AD clinical continuum; (4) assessment of the JPM in mesial temporal subregions known to be affected by early tau pathology. While strongly correlated in cortical regions, previous head-to-head studies comparing [^{18}F]flortaucipir and [^{18}F]RO948[27] and [^{18}F]GTP1 with [^{18}F]PI-2620 and [^{18}F]MK-6240[59]

have shown modest correlations in the hippocampus, most likely due to choroid plexus uptake; (5) interpretation of the CTR-100 values in larger cohorts to confirm that a value of 100 is indeed representative of younger (< 75) mild AD cases across all the tracers; (6) confirm the range of CTR values across AD patients varying in their severity of tau burden to understand where a CTR value of 100 fits; and (7) evaluate how to link CTR values to tau pathology using autopsy data, visual reads and large samples of individuals spanning the AD clinical continuum. JPM-based equations to convert SUVR to CTRs for the tau tracers included here will be forthcoming in subsequent work once the proposed validation has been completed.

AFFILIATIONS

[1]Clinical Memory Research Unit, Department of Clinical Sciences, Lund University, Lund, Sweden

[2]Critical Path for Alzheimer's Disease (CPAD) Consortium, Critical Path Institute, Tucson, Arizona, USA

[3]Enigma Biomedical Group, Knoxville, Tennessee, USA

[4]Eli Lilly and Company, Indianapolis, Indiana, USA

[5]Department of Neurology, University of Pittsburgh School of Medicine, Pittsburgh, Pennsylvania, USA

[6]Florey Department of Neuroscience, University of Melbourne, Parkville, Victoria, Australia

[7]Department of Molecular Imaging & Therapy, Austin Health, Heidelberg, Victoria, Australia

[8]F. Hoffmann-La Roche Ltd, Basel, Switzerland

[9]Clinical Imaging Group, Genentech, Inc., South San Francisco, California, USA

[10]Lawrence Berkeley National Laboratory, Berkeley, California, USA

[11]Janssen Research & Development, Merryfield Row San Diego, California, USA

[12]Life Molecular Imaging GmbH, Berlin, Germany

[13]Department of Radiology, University of Pittsburgh School of Medicine, Pittsburgh, Pennsylvania, USA

[14]Ace Alzheimer Center Barcelona, Universitat Internacional de Catalunya, Barcelona, Spain

[15]Networking Research Center on Neurodegenerative Diseases (CIBERNED), Instituto de Salud Carlos III, Av. de Monforte de Lemos, Madrid, Spain

[16]Wisconsin Alzheimer's Disease Research Center, University of Wisconsin-Madison School of Medicine and Public Health, Madison, Wisconsin, USA

[17]Department of Medicine Division of Geriatrics, University of Wisconsin-Madison School of Medicine and Public Health, Madison, Wisconsin, USA

[18]Department of Medical Physics, University of Wisconsin-Madison, School of Medicine and Public Health, Madison, Wisconsin, USA

[19]Eisai, Inc., Nutley, New Jersey, USA

[20]Biogen, Cambridge, Massachusetts, USA

[21]Invicro, Hammersmith Hospital, London, UK

[22]Brain Sciences, Imperial College London, Hammersmith Hospital, London, UK

[23]Department of Functional Brain Imaging, Institute for Quantum Medical Science, National Institutes for Quantum Science and Technology, Inage-ku, Chiba-shi, Chiba, Japan

[24]Merck & Co., Inc, West Point, Pennsylvania, USA

[25]Department of Psychiatry and Behavioral Sciences, University of California, San Francisco, California, USA

[26]Department of Neurology, Mayo Clinic, Rochester, Minnesota, USA

[27]University of California Berkeley, Lawrence Berkeley National Laboratory, Berkeley, California, USA

[28]Harvard Medical School, Department of Radiology, Boston, Minnesota, USA

[29]Gordon Center for Medical Imaging, Massachusetts General Hospital, Boston, Minnesota, USA

[30]Amsterdam University Medical Center, Neuroscience Campus Amsterdam, Alzheimercenter, HZ Amsterdam, the Netherlands

[31]Department of Psychology, Helen Wills Neuroscience Institute, University of California, Berkeley, California, USA

[32]Department of Neurology, VA Northern California Health Care System, Martinez, California, USA

[33]Department of Radiology, Mayo Clinic, Rochester, Minnesota, USA

[34]Department of Neurology, Memory and Aging Center, Weill Institute for Neurosciences, University of California, San Francisco, California, USA

[35]Department of Radiology & Biomedical Imaging, University of California, San Francisco, California, USA

[36]Translational Neuroimaging Laboratory, Department of Neurology and Neurosurgery, Faculty of Medicine, The McGill University Research Centre for Studies in Aging, McGill University, Verdun, Quebec, Canada

[37]Montreal Neurological Institute, McGill University, Montréal, Québec, Canada

[38]Department of Neurology, Skåne University Hospital, Lund, Sweden

[39]Alzheimer's Association, Chicago, Illinois, USA

[40]Senior advisor to CPAD Consortium, Critical Path Institute, Tucson, Arizona, USA

[41]The Australian Dementia Network (ADNeT), The University of Melbourne, Parkville, Victoria, Australia

[42]Memory Clinic, Skåne University Hospital, Malmö, Sweden

[43]Health and Biosecurity Flagship, The Australian eHealth Research Centre, CSIRO, Parkville, Victoria, Australia

ACKNOWLEDGMENTS

Support for the Critical Path Institute's CPAD Consortium comes from membership fees paid by members of the CPAD Consortium (https://c-path.org/programs/cpad/). Critical Path Institute is supported by the Food and Drug Administration (FDA) of the Department of Health and Human Services (HHS) and is 55% funded by the FDA/HHS, totaling $17,612,250, and 45% funded by non-government source(s), totaling $14,203,111. Work at Lund University has been funded by Swedish Research Council (2022-00775), ERA PerMed (ERAPERMED2021-184), the Knut and Alice Wallenberg foundation (2017-0383), the Strategic Research Area MultiPark (Multidisciplinary Research in Parkinson's disease) at Lund University, the Swedish Alzheimer Foundation (AF-980907), the Swedish Brain Foundation (FO2021-0293), The Parkinson foundation of Sweden (1412/22), the Cure Alzheimer's fund, the Konung Gustaf V:s och Drottning Victorias Frimurarestiftelse, the Skåne University Hospital Foundation (2020-O000028), Regionalt Forskningsstöd (2022-1259) and the Swedish federal government under the ALF agreement (2022-Projekt0080). GDR funding (not related to current work) – NIH/NIA P30-AG062422, U01 AG057195, R35 AG072362; Alzheimer's Association, ZEN-21-848216, American College of Radiology, Rainwater Charitable Foundation, Alliance for Therapeutics in Neurodegeneration.

CONFLICT OF INTEREST STATEMENT

Antoine Leuzy, Nicholas C. Cullen, Yashmin Karten, and Sudhir Sivakuraman reported that their organization (Critical Path Institute) received research funding via membership fees paid by members of the Critical Path for Alzheimer's Disease (CPAD) Consortium outside the submitted work. The contents are those of the author(s) and do not necessarily represent the official views of, nor an endorsement by, FDA/HHS or the U.S. Government. Lars Lau Raket, Emily C. Collins, Leonardo Iaccarino, Michael J. Pontecorvo, and Mark A. Mintun are full-time employees of Eli Lilly. Gregory Klein and Matteo Tonietto are full-time employees of Hoffmann-La Roche Ltd. Emily Olafson and Sandra Sanabria Bohorquez are full-time employees of Genentech, Inc. Ziad Saad is a full-time employees of Janssen. Antoine Leuzy, Samantha Budd Haeberlein and Hartmuch C. Kolb are consultants to Enigma Biomedical Group. Sulantha Mathotaarachchi is a full-time employee of Enigma Biomedical Group (Enigma Biomedical Group). Roger Gunn and Alex Whittington are full-time employees of Invicro. Maria C. Carillo is a full-time employee of the Alzheimer's Association. Santiago Bullich and Andrew Stephen are full-time employees of Life Molecular Imaging GmbH. Arnaud Charil and Michael C. Irizarry are full-time employees of Eisai. Jessica A. Collins and R. Matthew Hutchison are full-time employees of Biogen. Eric Hostetler is a full-time employee of Merck & Co., Inc. Victor L. Villemagne has received research grants from NHMRC (GNT2001320), the Aging Mind Foundation (DAF2255207), and NIH 2P01AG025204-16) and is and has been a consultant or paid speaker at sponsored conference sessions for Eli Lilly, Life Molecular Imaging, Ace Barcelona, BRI Japan, and AC Immune. Makoto Higuchi has received research grants from JST (JPMJMS2024) and AMED (20dm0207072) and holds patents on florzolotau and related compounds (JP 5422782/EP 12 884742.3/US 11667628/CA 2894994/HK 1208672), and the license of the patent rights has been granted to APRINOIA Therapeutics. Gil D. Rabinovici has received research support from Avid Radiopharmaceuiticals, GE Healthcare, Life Molecular Imaging, Genentech. Consulting fees from Alector, Eli Lilly, Johnson & Johnson, Merck, and is the Associate Editor for JAMA Neurology. Ruben Smith has received a speaker fee from Roche. Oskar Hansson has acquired research support (for the institution) from ADx, AVID Radiopharmaceuticals, Biogen, Eli Lilly, Eisai, Fujirebio, GE Healthcare, Pfizer, and Roche. In the past 2 years, he has received consultancy/speaker fees from AC Immune, Amylyx, Alzpath, BioArctic, Biogen, Cerveau, Eisai, Eli Lilly, Fujirebio, Merck, Novartis, Novo Nordisk, Roche, Sanofi, and Siemens. Marta Marquié has received funding support from Instituto de Salud Carlos III (ISCIII) Acción Estratégica en Salud, integrated in the Spanish National RCDCI Plan and financed by ISCIII-Subdirección General de Evaluación and the Fondo Europeo de Desarrollo Regional (FEDER—Una manera de hacer Europa) grant PI19/00335, has received travel support to attend scientific meeting from F. Hoffmann-La Roche Ltd, and has participated in the Spanish Scientific Advisory Board of Biomarkers of Araclon Biotech-Grífols. Mercè Boada has received consultancy fees from Grifols, Araclon Biotech, Roche, Biogen, Eli Lilly, Merck, Zambon, and Novo-Nordisk. Billy Dunn is a consultant for ArchVenture Partners, Cerveau Technologies, Epilepsy Foundation, F-PRIME Capital, Loulou Foundation, and Michael J. Fox Foundation. He has served as president of the Virginia Neurological Society and is director of Prothena Inc. Keith Johnson is a consultant for Novartis and Merck. Sterling Johnson is a consultant for Enigma Biomedical Group and Alzpath. The other authors did not report any conflict of interest. Author disclosures are available in the supporting information.

CONSENT STATEMENT

Ethics approval was provided by the universities' institutional review boards. All participants provided written informed consent.

REFERENCES

1. Savva GM, Wharton SB, Ince PG, et al. Age, neuropathology, and dementia. *N Engl J Med*. 2009;360:2302-2309.
2. Sintini I, Graff-Radford J, Senjem ML, et al. Longitudinal neuroimaging biomarkers differ across Alzheimer's disease phenotypes. *Brain*. 2020;143:2281-2294.
3. Ossenkoppele R, Schonhaut DR, Scholl M, et al. Tau PET patterns mirror clinical and neuroanatomical variability in Alzheimer's disease. *Brain*. 2016;139:1551-1567.
4. Iaccarino L, La Joie R, Edwards L, et al. Spatial relationships between molecular pathology and neurodegeneration in the Alzheimer's disease continuum. *Cereb Cortex*. 2021;31:1-14.
5. Bejanin A, Schonhaut DR, La Joie R, et al. Tau pathology and neurodegeneration contribute to cognitive impairment in Alzheimer's disease. *Brain*. 2017;140:3286-5300.
6. Harrison TM, Du R, Klencklen G, Baker SL, Jagust WJ. Distinct effects of beta-amyloid and tau on cortical thickness in cognitively healthy older adults. *Alzheimers Dement*. 2021;17:1085-1096.
7. Johnson KA, Schultz A, Betensky RA, et al. Tau positron emission tomographic imaging in aging and early Alzheimer disease. *Ann Neurol*. 2016;79:110-119.
8. Ossenkoppele R, Smith R, Ohlsson T, et al. Associations between tau, Abeta, and cortical thickness with cognition in Alzheimer disease. *Neurology*. 2019;92:e601-e612.
9. Scholl M, Lockhart SN, Schonhaut DR, et al. PET imaging of tau deposition in the aging human brain. *Neuron*. 2016;89:971-982.
10. Ossenkoppele R, Pichet Binette A, Groot C, et al. Amyloid and tau PET-positive cognitively unimpaired individuals are at high risk for future cognitive decline. *Nat Med*. 2022;28:2381-2387.
11. Ossenkoppele R, Smith R, Mattsson-Carlgren N, et al. Accuracy of tau positron emission tomography as a prognostic marker in preclinical and prodromal Alzheimer disease: a head-to-head comparison against amyloid positron emission tomography and magnetic resonance imaging. *JAMA Neurol*. 2021;78:961-971.
12. Klunk WE, Engler H, Nordberg A, et al. Imaging brain amyloid in Alzheimer's disease with Pittsburgh Compound-B. *Ann Neurol*. 2004;55:306-319.
13. Pemberton HG, Collij LE, Heeman F, et al. Quantification of amyloid PET for future clinical use: a state-of-the-art review. *Eur J Nucl Med Mol Imaging*. 2022;49:3508-3528.
14. Leuzy A, Chiotis K, Lemoine L, et al. Tau PET imaging in neurodegenerative tauopathies-still a challenge. *Mol Psychiatry*. 2019;24:1112-1134.
15. Jie C, Treyer V, Schibli R, Mu L. Tauvid: the first FDA-approved PET tracer for imaging tau pathology in Alzheimer's disease. *Pharmaceuticals (Basel)*. 2021:14.
16. Cummings J. The role of biomarkers in Alzheimer's disease drug development. *Adv Exp Med Biol*. 2019;1118:29-61.
17. Villemagne VL, Lopresti BJ, Dore V, et al. What is T+? A Gordian knot of tracers, thresholds, and topographies. *J Nucl Med*. 2021;62:614-619.
18. Klunk WE. Molecular imaging: what is right and what is an illusion? *Alzheimers Dement (Amst)*. 2018;10:217-220.

19. Klunk WE, Koeppe RA, Price JC, et al. The Centiloid Project: standardizing quantitative amyloid plaque estimation by PET. *Alzheimers Dement*. 2015;11:1-15.
20. La Joie R, Ayakta N, Seeley WW, et al. Multisite study of the relationships between antemortem [(11)C]PIB-PET Centiloid values and postmortem measures of Alzheimer's disease neuropathology. *Alzheimers Dement*. 2019;15:205-216.
21. Su Y, Flores S, Hornbeck RC, et al. Utilizing the Centiloid scale in cross-sectional and longitudinal PiB PET studies. *Neuroimage Clin*. 2018;19:406-416.
22. Klein G, Delmar P, Voyle N, et al. Gantenerumab reduces amyloid-beta plaques in patients with prodromal to moderate Alzheimer's disease: a PET substudy interim analysis. *Alzheimers Res Ther*. 2019;11:101.
23. Shcherbinin S, Evans CD, Lu M, et al. Association of amyloid reduction after donanemab treatment with tau pathology and clinical outcomes: the TRAILBLAZER-ALZ randomized clinical trial. *JAMA Neurol*. 2022;79:1015-1024.
24. Karran E, De Strooper B. The amyloid hypothesis in Alzheimer disease: new insights from new therapeutics. *Nat Rev Drug Discov*. 2022;21:306-518.
25. Karpen SR, White JK, Mullin AP, et al. Effective data sharing as a conduit for advancing medical product development. *Ther Innov Regul Sci*. 2021;55:591-600.
26. Villemagne VL, Leuzy A, Bohorquez SS, et al. CenTauR: toward a universal scale and masks for standardizing tau imaging studies. *Alzheimers Dement (Amst)*. 2023;15:e12454.
27. Smith R, Scholl M, Leuzy A, et al. Head-to-head comparison of tau positron emission tomography tracers [(18)F]flortaucipir and [(18)F]RO948. *Eur J Nucl Med Mol Imaging*. 2020;47:342-354.
28. Gogola A, Minhas DS, Villemagne VL, et al. Direct comparison of the tau PET tracers (18)F-Flortaucipir and (18)F-MK-6240 in Human Subjects. *J Nucl Med*. 2022;63:108-116.
29. Rodriguez-Gomez O, Sanabria A, Perez-Cordon A, et al. FACEHBI: a prospective study of risk factors, biomarkers and cognition in a cohort of individuals with subjective cognitive decline. study rationale and research protocols. *J Prev Alzheimers Dis*. 2017;4:100-108.
30. Amadoru S, Dore V, McLean CA, et al. Comparison of amyloid PET measured in Centiloid units with neuropathological findings in Alzheimer's disease. *Alzheimers Res Ther*. 2020;12:22.
31. Jack CR Jr, Bennett DA, Blennow K, et al. NIA-AA Research Framework: toward a biological definition of Alzheimer's disease. *Alzheimers Dement*. 2018;14:535-562.
32. Shuping JL, Matthews DC, Adamczuk K, et al. Development, initial validation, and application of a visual read method for [(18)F]MK-6240 tau PET. *Alzheimers Dement (N Y)*. 2023;9:e12372.
33. Seibyl JP, DuBois JM, Racine A, et al. A visual interpretation algorithm for assessing brain tauopathy with (18)F-MK-6240 PET. *J Nucl Med*. 2023;64:444-451.
34. Fleisher AS, Pontecorvo MJ. Positron emission tomography imaging with [18F]flortaucipir and postmortem assessment of Alzheimer disease neuropathologic changes. *JAMA Neurol*. 2020;77:829-839.
35. Smith R, Hagerstrom D, Pawlik D, et al. Clinical utility of tau positron emission tomography in the diagnostic workup of patients with cognitive symptoms. *JAMA Neurol*. 2023;80:749-756.
36. Sonni I, Lesman Segev OH, Baker SL, et al. Evaluation of a visual interpretation method for tau-PET with (18)F-flortaucipir. *Alzheimers Dement (Amst)*. 2020;12:e12133.
37. Braak H, Alafuzoff I, Arzberger T, Kretzschmar H, Del Tredici K. Staging of Alzheimer disease-associated neurofibrillary pathology using paraffin sections and immunocytochemistry. *Acta Neuropathol*. 2006;112:389-404.
38. Braak H, Braak E. Neuropathological stageing of Alzheimer-related changes. *Acta Neuropathol*. 1991;82:239-259.
39. Janelidze S, Zetterberg H, Mattsson N, et al. CSF Abeta42/Abeta40 and Abeta42/Abeta38 ratios: better diagnostic markers of Alzheimer disease. *Ann Clin Transl Neurol*. 2016;3:154-165.
40. Pontecorvo MJ, Devous MD, Kennedy I, et al. A multicentre longitudinal study of flortaucipir (18F) in normal ageing, mild cognitive impairment and Alzheimer's disease dementia. *Brain*. 2019;142:1723-1735.
41. Scholl M, Ossenkoppele R, Strandberg O. Distinct 18F-AV-1451 tau PET retention patterns in early- and late-onset Alzheimer's disease. *Brain*. 2017;140:2286-2294.
42. Rowe CC, Doré V, Krishnadas N, et al. Tau Imaging with 18F-MK6240 across the Alzheimer's Disease spectrum. *MedRxiV*. 2022. doi:10.1101/2022.02.13.22270894
43. Dore V, Krishnadas N, Bourgeat P, et al. Relationship between amyloid and tau levels and its impact on tau spreading. *Eur J Nucl Med Mol Imaging*. 2021;48:2225-2232.
44. Baker SL, Maass A, Jagust WJ. Considerations and code for partial volume correcting [(18)F]-AV-1451 tau PET data. *Data Brief*. 2017;15:648-657.
45. Kristensen K, Nielsen A, Berg CW, Skaug H, Bell BM. TMB: automatic differentiation and laplace approximation. *J Stat Softw* . 2016;70(5):1-21.
46. Schwarz CG, Tosakulwong N, Senjem ML, et al. Considerations for performing level-2 centiloid transformations for amyloid PET SUVR values. *Sci Rep*. 2018;8:7421.
47. Krishnadas N, Dore V, Robertson JS, et al. Rates of regional tau accumulation in ageing and across the Alzheimer's disease continuum: an AIBL (18)F-MK6240 PET study. *EBioMedicine*. 2023;88:104450.
48. Leuzy A, Binette AP, Vogel JW, et al. Comparison of group-level and individualized brain regions for measuring change in longitudinal tau positron emission tomography in Alzheimer disease. *JAMA Neurol*. 2023;80:614-623.
49. Vogel JW, Young AL, Oxtoby NP, et al. Four distinct trajectories of tau deposition identified in Alzheimer's disease. *Nat Med*. 2021;27:871-881.
50. Krishnadas N, Huang K, Schultz SA, et al. Visually identified tau 18F-MK6240 PET patterns in symptomatic Alzheimer's disease. *J Alzheimers Dis*. 2022;88:1627-1637.
51. Schmidt ME, Chiao P, Klein G, et al. The influence of biological and technical factors on quantitative analysis of amyloid PET: points to consider and recommendations for controlling variability in longitudinal data. *Alzheimers Dement*. 2015;11:1050-1068.
52. Gogola AMD, Lopresti B, et al., Considerations for a Universal Tau PET Reference Region. Tau 2022 Global Conference; 2022.
53. Janelidze S, Pannee J, Mikulskis A, et al. Concordance between different amyloid immunoassays and visual amyloid positron emission tomographic assessment. *JAMA Neurol*. 2017;74(12):1492-1501. doi:10.1001/jamaneurol.2017.2814
54. Heurling K, Smith R, Strandberg OT, et al. Regional times to equilibria and their impact on semi-quantification of [(18)F]AV-1451 uptake. *J Cereb Blood Flow Metab*. 2019;39(11):2223-2232. doi:10.1177/0271678×18791430
55. Honhar P, Matuskey D, Carson RE, Hillmer AT. Improving SUVR quantification by correcting for radiotracer clearance in tissue. *J Cereb Blood Flow Metab*. 2023;44(2):296-309. doi:10.1177/0271678×231196804
56. Mohanraj P, Carson RE, Hillmer AT, Honhar P, Bridging the gap between SUVR and DVR for [18F]MK6240 by correcting for tracer clearance in tissue: a simulation study. Presented at the Human Amyloid Imaging Conference, Miami, Florida, January 17-19, 2024.
57. Cho H, Mundada NS, Apostolova LG, et al. Amyloid and tau-PET in early-onset AD: baseline data from the Longitudinal Early-onset Alzheimer's Disease Study (LEADS). *Alzheimers Dement*. 2023;19(Suppl 9):S98-S114.

58. Bauer-Negrini G, Povala G, Amaral L, et al., Universal scale for tau PET based on head-to-head data: the HEAD study. Presented at the Human Amyloid Imaging Conference, Miami, Florida, January 16-19 2024.
59. Tonietto M, Constantinescu C, Sanabria Bohorquez S, et al., In Vivo Head-To-Head Comparison of [18F]GTP1, [18F]PI2620, and [18F]MK6240 in Alzheimer's Disease. Presented at the Human Amyloid Imaging Conference, Miami, Florida, January 11-13, 2023.

SUPPORTING INFORMATION

Additional supporting information can be found online in the Supporting Information section at the end of this article.

How to cite this article: Leuzy A, Raket LL, Villemagne VL, et al. Harmonizing tau positron emission tomography in Alzheimer's disease: The CenTauR scale and the joint propagation model. *Alzheimer's Dement*. 2024;20:5833–5848. https://doi.org/10.1002/alz.13908